11 T Twin-Aperture Nb_3Sn Dipole Development for LHC Upgrades

A.V. Zlobin, N. Andreev, G. Apollinari, B. Auchmann, E. Barzi, S. Izquierdo Bermudez, R. Bossert, M. Buehler, G. Chlachidze, J. DiMarco, M. Karppinen, F. Nobrega, I. Novitski, L. Rossi, D. Smekens, M. Tartaglia, D. Turrioni, G. Velev

***Abstract*— FNAL and CERN are developing a twin-aperture 11 T Nb_3Sn dipole suitable for installation in the LHC. This paper describes the design and parameters of the 11 T dipole developed at FNAL for the LHC upgrades in both single-aperture and twin-aperture configurations, and presents details of the constructed dipole models. Results of studies of magnet quench performance, quench protection and magnetic measurements performed using short 1 m long coils in the dipole mirror and single-aperture configurations are reported and discussed.**

***Index Terms*— Accelerator magnets, Large Hadron Collider, superconducting coils, magnet design, quench protection.**

I. Introduction

THE PLANNED upgrades of the Large Hadron Collider (LHC) call for additional collimators in the dispersion suppressor (DS) areas around points 2, 3, 7, and CMS and ATLAS detectors [1]. The necessary space for these devices could be provided by replacing some 8.33 T 15 m long Nb-Ti LHC main dipoles (MB) with shorter 11 T Nb_3Sn dipoles (MBH) compatible with the LHC lattice and main systems, and delivering the same integrated strength of 119 Tm at the operation current of 11.85 kA. To validate the viability of this approach, CERN and FNAL magnet groups are conducting a joint R&D program intended to develop a 5.5 m long twin-aperture 11 T Nb_3Sn dipole prototype. Two of these magnets with a collimator in between will replace one MB dipole.

As a first stage of the program, the 2 m long single-aperture Nb_3Sn dipole demonstrator MBHSP01 [2] was developed, fabricated and tested at FNAL in June 2012. The magnet reached 10.4 T at the LHC operating temperature of 1.9 K [3]. This test revealed considerable conductor degradation in the coil that instigated instabilities and spontaneous quenches during the current plateau at currents above 8 kA. To improve the magnet design and fabrication process, quench performance and field quality, and demonstrate performance reproducibility, the fabrication of eight 1 m long coils was started at FNAL in the middle of 2012. Four coils were collared and tested first in a single-aperture configuration (MBHSP02 and MBHSP03) prior to their assembly and test inside a common iron yoke (twin-aperture configuration) [4]. One coil, equipped with additional instrumentation, was tested in a dipole mirror structure [5] to assess the effect of coil design and preload on the magnet quench performance, and perform quench protection studies.

This paper describes the design and parameters of the 11 T Nb_3Sn dipole developed at FNAL for the LHC upgrades and presents details of the constructed coils and dipole models. Results of studies of magnet quench performance, quench protection and magnetic measurement performed using short 1 m long coils in dipole mirror and single-aperture configurations are reported and discussed.

II. Magnet Design and Parameters

Design concepts of the 11 T Nb_3Sn dipole for LHC upgrades in both single-aperture and twin-aperture configurations are described in [2], [6]. The dipole design features 2-layer shell-type Nb_3Sn coils, separate stainless steel collars for each aperture and the MB yoke modified in the area of the collar yoke interface. The magnet coil was designed to provide a dipole field of 11 T in a 60 mm aperture at the LHC nominal operation current of 11.85 kA with 20% margin along the load line, and low-order geometrical field harmonics below 10^{-4} inside the 34 mm diameter circle. The chosen coil aperture of 60 mm is slightly larger than the MB dipole aperture, which avoids bending the Nb_3Sn coils in order to accommodate the LHC beam sagitta. Using separate collars for each aperture simplifies magnet assembly, reduces the risk of coil damage during assembly and allows testing collared coils in both single-aperture and twin-aperture configurations. Fig. 1 shows the cross-sections of the coil and the 11 T dipole magnet (FNAL design) in both configurations.

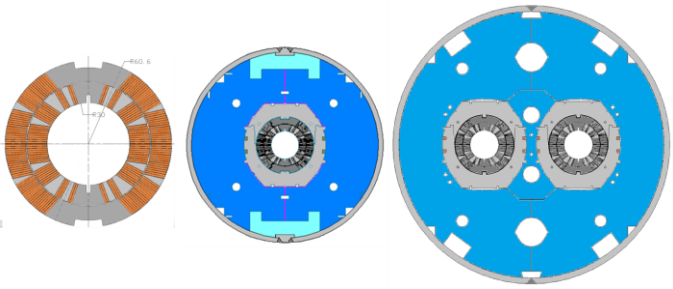

Fig. 1. The 2-layer coil (left), and single-aperture (middle) and twin-aperture (right) dipole configurations.

Manuscript received August 12, 2014. Work supported by Fermi Research Alliance, LLC, under contract No. DE-AC02-07CH11359 with the U.S. Department of Energy and European Commission under FP7 project HiLumi LHC, GA no. 284404.

N. Andreev, G. Apollinari, E. Barzi, R. Bossert, M. Buhler, G. Chlachidze, J. DiMarco, F. Nobrega, I. Novitski, M. Tartaglia, D. Turrioni, A.V. Zlobin, G. Velev are with Fermi National Accelerator Laboratory, P.O. Box 500, Batavia, IL 60510, USA (phone: 630-840-8192; e-mail: zlobin@fnal.gov).

B. Auchmann, S. Izquierdo Bermudez, M. Karppinen, L. Rossi, D. Smekens are with the European Organization for Nuclear Research, CERN CH-1211, Genève 23, Switzerland.

The mechanical structure and the coil pre-stress of the 11 T dipole were optimized to keep the coil stress below 165 MPa during magnet assembly and operation. ANSYS analysis shows that this pre-stress level is sufficient to keep the coils under compression up to the ultimate design field of 12 T [6].

The 11 T dipole design parameters calculated for long single-aperture and twin-aperture configurations at the LHC nominal operation current of 11.85 kA, the operation temperature of 1.9 K, the strand critical current density $J_c(12T,4.2K)$=2750 A/mm^2, the Cu/nonCu ratio of 1.1, and the cable critical current degradation of 10% are shown in Table I.

TABLE I
11 T DIPOLE PARAMETERS AT I_{NOM}.

Parameter	Single-aperture	Twin-aperture
Yoke outer diameter, mm	400	550
Nominal bore field at I_{nom}, T	10.88	11.23
Short sample field B_{SSL} at T_{op}, T	13.4	13.9
Margin B_{nom}/B_{SSL} at T_{op}, %	81	83
Stored energy at I_{nom}, kJ/m	424	969
F_x/quadrant at I_{nom}, MN/m	2.89	3.16
F_y/quadrant at I_{nom}, MN/m	-1.58	-1.59

III. SINGLE-APERTURE MODELS

Following the fabrication and test of dipole demonstrator MBHSP01, the short model R&D at FNAL was focused on further optimization of the strand, cable and coil designs and fabrication processes, coil assembly and pre-load including collaring, yoking and skinning steps, as well as on quench performance, protection, field quality, and performance reproducibility studies.

The 11 T dipole uses a Rutherford cable with 40 Nb_3Sn strands 0.7 mm in diameter. The optimization of strand and cable parameters was focused on the strand architecture (sub-element number, size and distribution in the cross-section), cable cross-section, cable compaction and I_c degradation, stainless steel (SS) core size and Residual Resistivity Ratio (RRR) of the copper matrix. Results of the strand and cable study and optimization for the 11 T program at FNAL are reported in [7], [8]. The cross-sections of two strand types, used in short coils, and the cored cable are shown in Fig. 2.

The dipole coil consists of 2 layers, 6 blocks and 56 turns. Both layers are wound from a single piece of cable insulated with a 0.075 mm thick and 12.7 mm wide E-glass tape with ~50% overlap. The coil fabrication process is based on the wind-and-react method. After reaction coils are impregnated with epoxy resin. The titanium-alloy coil poles, and stainless steel wedges and end parts are glued into the coil during the epoxy impregnation. The details of the coil fabrication process are reported in [9]. The picture and the coil cross-section of an impregnated coil are shown in Fig. 3.

The collared coil consists of two coils, a multilayer Kapton ground insulation, stainless steel protection shells, and stainless steel collar blocks locked on each side by two bronze keys. Two quench protection heaters are mounted on each side of the coil between the 1st and 2nd Kapton layers of the ground insulation. Collar laminations and a collared coil assembly are shown in Fig. 4.

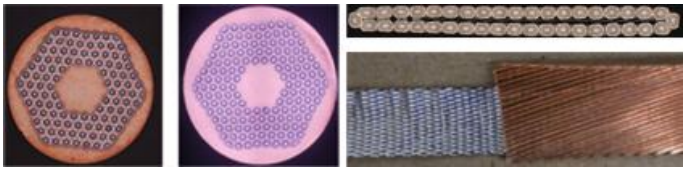

Fig. 2. RRP108/127 and RRP150/169 strands and 40-strand cored cable.

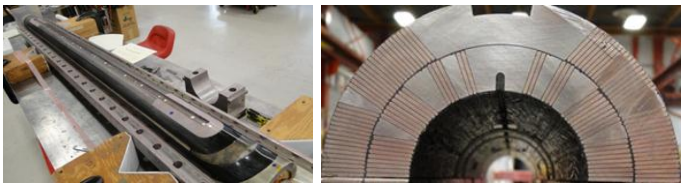

Fig. 3. Impregnated coil (left) and coil cross-section (right).

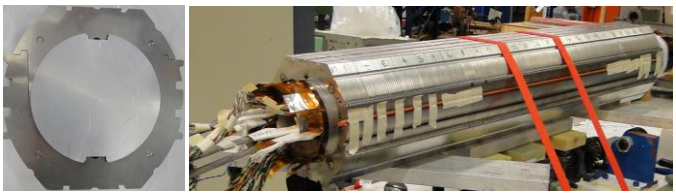

Fig. 4. Stainless steel collars (left) and collared coil assembly (right).

Eight 1 m long coils (#5-#12) were fabricated at FNAL since the middle of 2012. Coil #6 was damaged during curing. Coils #5, #7, #9 and #10 were used in two collared coil assemblies tested in a single-aperture configuration (MBHSP02 and MBHSP03). These collared coils are being used in the first twin-aperture dipole model MBHDP01. Coil #8 was heavily instrumented and tested in a dipole mirror configuration (MBHSM01) to study the effect of coil pre-stress and to measure quench protection parameters [10]. Coils #11 and #12 will be tested first in the single-aperture configuration MBHSP04 and then used in the 2nd twin-aperture dipole model.

Design features of the 1-m long coils and single-aperture models are shown in Table II. The coils used three end spacer design modifications: the original (v.1), with shortened legs (v.2), and with flexible legs developed at CERN (v.3) [11]. The models were assembled with two collar modifications and two collar-yoke mid-plane shims. The v.2 collar had a slightly larger inner radius for a thicker protection shell.

TABLE II
MODEL DESIGN FEATURES

Model	Coil #	Strand	Coil	Collar	Mid-plane shim
MBHSP02	5 7	RRP-150/169	End spacers v.1	Laser-cut collar v.1	0.24 mm*
MBHSM01	8	RRP-108/127	-"-	No collar	0.0 mm**
MBHSP03	9 10	-"-	End spacers v.2	Stamped collar v.2	0.1 mm*
MBHSP04	11 12	-"-	End spacers v.3	-"-	TBD

* Collar-yoke mid-plane shim
** Coil-yoke mid-plane shim

The cross-sections of the short dipole model and dipole mirror structure with a 400 mm diameter iron yoke, aluminum clamps, and 12 mm thick bolt-on stainless steel skin are shown in Fig. 5. Two 50 mm thick stainless steel end plates, bolted to the skin, restrict the coil axial motion through a pair of instrumented bullets per coil end.

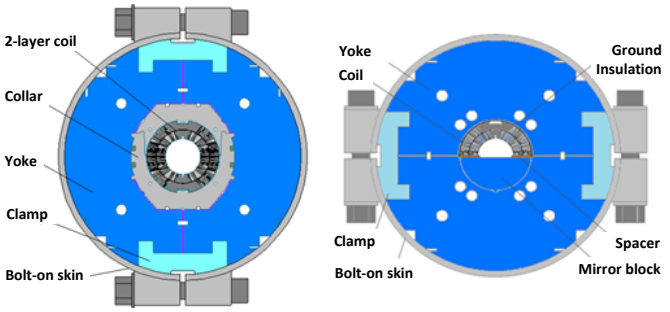

Fig. 5. Cross-sections of the 11 T dipole (left) and the dipole mirror (right).

IV. Quench Performance

The magnets were tested at the FNAL Vertical Magnet Test Facility in the following order: MBHSP02 (May-June 2013), MBHSM01 (December 2013-January 2014) and MBHSP03 (April-May 2014). The coils were instrumented with voltage taps and a quench antenna to detect and localize quench origins. The magnet quench current (short sample) limits I_{SSL} and the maximum bore field B_{max}, estimated using witness sample data, are reported in Table III. For the mirror, B_{max} is the maximum field in the coil.

TABLE III
Short Sample Limits

	MBHSP02		MBHSP03		MBHSM01	
T (K)	4.5	1.9	4.5	1.9	4.5	1.9
I_{SSL} (kA)	14.3	16.0	13.2	15.1	13.0	14.5
B_{max} (T)	12.7	14.1	12.0	13.5	11.7*	12.9*

* B_{max} in coil

A. Magnet training

The training quenches of dipole models MBHSP02 and MBHSP03, and dipole mirror MBHSM01 at 4.5 K and 1.9 K are summarized in Fig. 6. The quench currents normalized to the magnet SSL at the corresponding temperatures are reported in Fig. 7. In all the plots the data at 4.5 K are represented with dark markers and the data at 1.9 K with light markers.

The magnet training process started at 4.5 K with a current ramp rate of 20 A/s. After slowing-down or reaching a plateau, training continued at 1.9 K. The first quench in all the magnets occurred at ~65% of the SSL, although the absolute values were slightly different and correlated with the magnet SSLs (see Table III). Despite the different strand design and critical current density, and the coil pre-stress level the relative values of the first 18 quenches at 4.5 K for both dipole models were very close. However, the training rate of the magnets at 1.9 K was quite different. MBHSP03 with low pole pre-stress was trained to ~80% of its SSL after 35 quenches whereas MBHSP02 with high pre-stress needed 65 quenches.

Dipole mirror MBHSM01 with reduced coil pole pre-stress was trained to 80% of the SSL after only 4 quenches and to almost 100% of the SSL at 4.5 and 1.9 K after 25 and 15 quenches, respectively. All training quenches in MBHSM01 started in the high field area of the coil inner layer, with only two quenches in the coil outer layer. The plateau quenches both at 1.9 and 4.5 K started in the segment, next to the 2nd wedge.

Unlike MBHSP01 and MBHSP02, dipole mirror MBHSM01 demonstrated stable performance during a 25 min long current plateau at 13 kA (90% of SSL) at 1.9 K and 12 kA (92% of SSL) at 4.5 K.

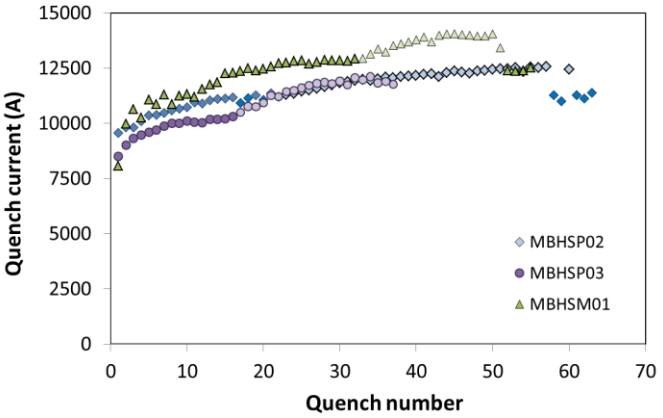

Fig. 6. MBHSM01, MBHSP02 and MBHSP03 training.

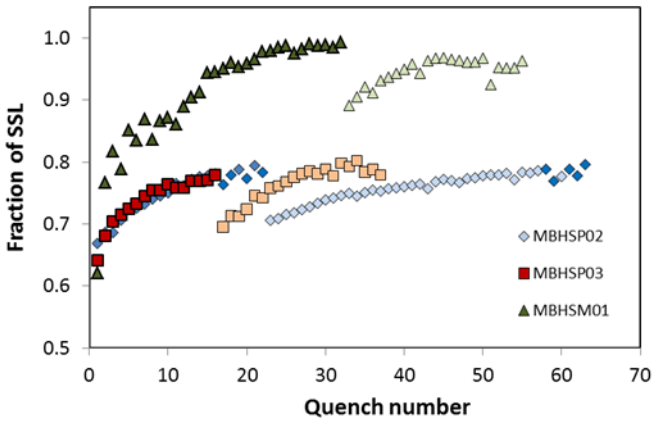

Fig. 7. Quench current normalized on magnet SSL.

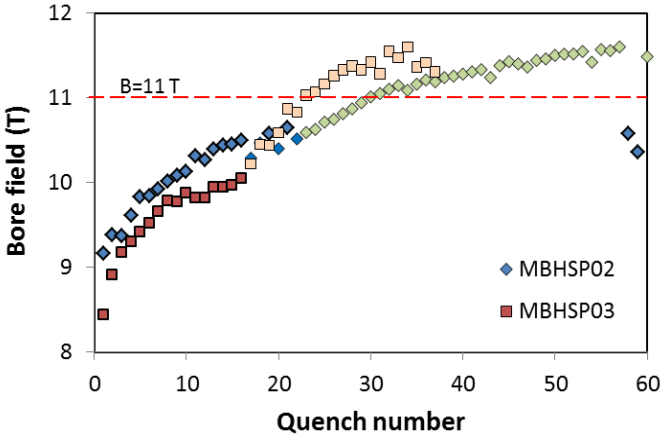

Fig. 8. Quench bore field during magnet training.

Since the design and fabrication process of coil #8 were the same as of coils #5 and #7, the improved quench performance of coil #8 in the dipole mirror structure suggested that the large mid-plane shim was likely a major cause of the conductor degradation in the dipole model MBHSP02. Therefore this shim in MBHSP03 was reduced to the level necessary to compensate for the difference in collar and yoke thermal contraction. As a result, in addition to more rapid training, no quenches were detected in MBHSP03 after ~30 min at steady currents up to the nominal LHC operation current. Fluctuations of quench currents, seen in MBHSP03, are likely due to epoxy cracking between the pole blocks and coil turns caused by the

low pole pre-stress in this model. To avoid possible conductor degradation magnet training was stopped.

Fig. 8 shows the bore field training for dipole models MBHSP02 and MBHSP03 using quench current data from Fig. 6 and the measured magnet transfer functions shown in Fig. 19. In MBHSP02 and MBHSP03 the bore field of 11 T was reached after 31 and 22 training quenches respectively. All the training quenches at the magnet temperature of 1.9 K occurred in the inner-layer high-field blocks. Both dipole models were trained to ~97% of the magnet design field of 12 T. Training will continue after assembly of these collared coils in a twin-aperture model.

B. *Ramp rate sensitivity*

Both dipole models MBHSP02 and MBHSP03, and dipole mirror MBHSM01 used cables with a stainless steel core to reduce the ramp rate sensitivity of magnet performance. The effect of the cable core on the ramp rate dependence of the magnet bore field at 1.9 K is demonstrated in Fig. 9 for MBHSP02. The ramp rate sensitivity of the magnet bore field is low as expected for a coil made of cored cable. Although during the current ramp up at dI/dt>50 A/s the magnet quenches below the nominal bore field of 11 T, no quenches were observed at 1.9 K when ramping the current down from 11 T field at the ramp rate of 200 A/s. Similar result was observed in dipole mirror MBHSM01 and is expected for dipole model MBHSP03.

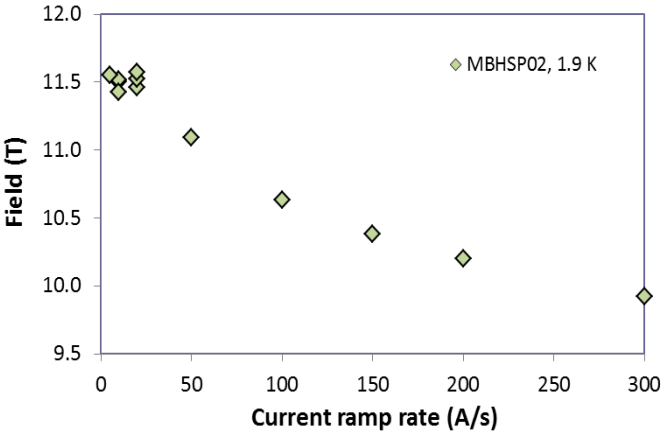

Fig. 9. Ramp rate dependence of MBHSP02 bore field at 1.9 K.

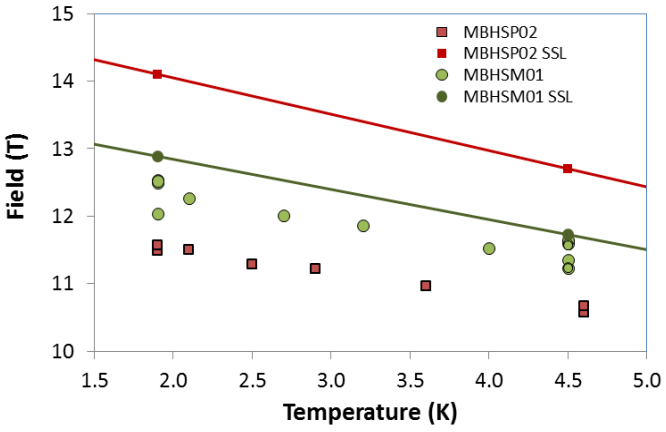

Fig. 10. Temperature dependence of MBHSP02 bore field and MBHSM01coil maximum field.

C. *Temperature margin*

Temperature dependence of a magnet maximum quench current provides information on the level and possible cause of conductor degradation in the magnet, and the value of a magnet minimal temperature margin. Note that due to the non-uniform field distribution, the local temperature margin varies inside the coil. Temperature dependences of the bore field in dipole model MBHSP02 and of the coil maximum field in dipole mirror MBHSM01, measured in the temperature range of 1.9-4.6 K, are shown in Fig. 10. The MBHSP02 and MBHSM01short sample limits are shown by solid lines.

Due to the conductor degradation in MBHSP02, the magnet quench field is ~18% lower than the SSL. However, the magnet temperature margin at the nominal operation field of 11 T at 1.9 K is still ~1.5 K in the coil high-field regions.

As shown earlier, MBHSM01 has reached its SSL with small conductor degradation. The 4% degradation of the magnet quench current during training at 1.9 K is seen in Figs. 6, 7 and 10. At this level of conductor degradation, the expected minimal temperature margin at the nominal field of 11 T is more than 3 K. Note that even at 4.5 K the dipole design allows operation at the nominal field of 11 T with ~5% field margin and more than 1 K temperature margin. Although the temperature dependence of MBHSP03 was not measured, a similar performance is expected for this magnet.

V. Quench Protection Study

Due to the large stored energy, the quench protection of the 11 T dipoles is a challenging problem. It was comprehensively studied at FNAL, including simulations [12], [13] and measurements using the short dipole models [14], and the dipole mirror [10]. Similar studies are being performed also at CERN [11], [15], [16]. In the dipole models quench protection studies were limited by currents close to the nominal operation current of ~12 kA or ~80% of magnet SSL. Due to the improved quench performance, quench protection studies in dipole mirror MBHSM01 were extended to currents up to 92% of the SSL.

For quench protection studies coil #8 was equipped with additional voltage taps, and regular protection and spot heaters. Two protection heaters (PH), composed of 0.025 mm thick stainless steel strips, were placed on the coil outer surface separated from the coil by a 0.127 mm thick Kapton layer of ground insulation and a 0.125 mm epoxy impregnated S2-glass wrap. The width of heater strips in the high field (HF) and low field (LF) coil blocks is 26 mm and 21.5 mm, respectively.

Spot heaters (SH) made of 2 mm wide stainless steel strip were mounted on the coil inner-layer (IL) and outer-layer (OL) mid-plane turns. Each SH, surrounded by two voltage taps, covers an area 32 mm long by 14 mm wide. Two voltage taps, separated by 10 cm, were installed next to the SH. Due to the IL spot heater wiring damage during the dipole mirror assembly, only the OL spot heater was available for testing.

A. *Minimum PH power density*

The minimum value of the PH peak power density $P_{AV,}$ required to quench the magnet, is a key parameter for the quench protection system design. Fig. 11 shows this parameter

for the 11 T dipole coil, measured and calculated as a function of the magnet current using the model described in [15]. Measurements and calculations show that to quench the magnet at the LHC operation currents from 0.76 to 11.85 kA, an average PH peak power density of 55 W/cm^2 is needed. Since the width of the LF and HF heater strips is slightly different, the minimum peak power density is also different in the LF and HF blocks of the coil outer layer:

$$P_{LF}=1.24 \cdot P_{AV} \text{ and } P_{HF}=P_{AV}/1.24,$$

where P_{AV} is the average peak power density for both heaters. Based on simulations and measurements (Fig. 18), the value of the minimum peak power density to quench the magnet is driven by the pole turns in the OL HF blocks.

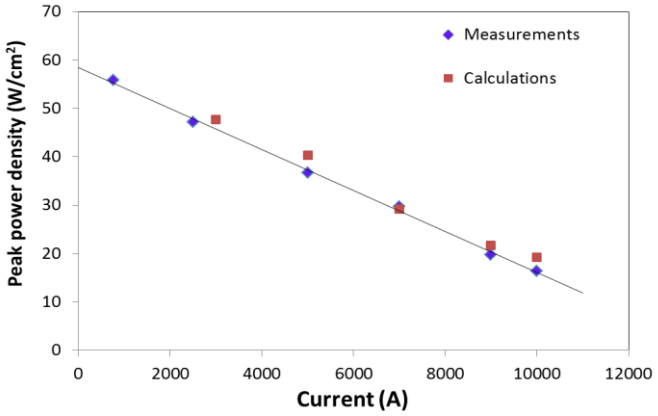

Fig. 11. Peak power density vs. magnet current at 4.5 K (MBHSP02).

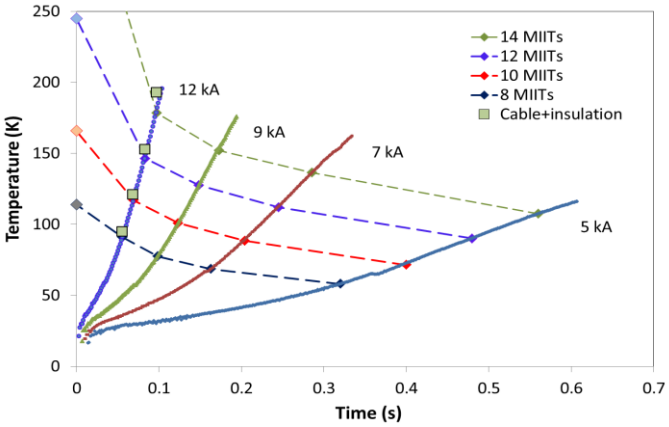

Fig. 12. Cable quench temperature vs. time (MBHSM01).

B. *Quench temperature measurements*

The coil maximum temperature in the case of a quench is estimated based on the Quench Integral (*QI*) calculated over the current decay time using the adiabatic approach. Simulations of quench processes show that the heat transfer from the cable inside the magnet coil plays an important role [12]. To measure the effect of heat transfer from the cable, the cable temperature growth in the coil due to a quench was measured using quenches at constant coil current induced by the spot heater. The coil temperature was determined using the measured voltage between the voltage taps near SH and the dependence of cable resistance vs. temperature [10].

The coil temperature as a function of time at fixed coil currents is shown in Fig. 12. The dashed lines connect the temperature points corresponding to the same *QI* values. The temperature points on the vertical axis (t=0) represent the adiabatic calculations for the corresponding bare cable. The dependence of the cable temperature not only on the value of *QI*, but also on the time during which it is accumulated, confirms the strong cable cooling effect in the coil. The adiabatic calculations for the insulated cable impregnated with epoxy represented by squares are in good agreement with measurements at I=12 kA at t=0.05-0.1 s. This is the time interval necessary to transfer the heat generated in the bare cable to the cable insulation. Transfer of heat to the cable insulation leads to substantial reduction of the cable temperature up to 40-50%. Since the quench time of an accelerator magnet is usually longer than 0.2 s, the effect of cable cooling is even stronger.

C. *Quench Integral*

The Quench Integral measured in MBHSM01 using protection heaters as a function of the magnet current for the external dump resistor R_d =0 is shown in Fig. 13. At the LHC nominal current of ~12 kA *QI is* ~15 MIITs. Based on the adiabatic calculations for the insulated cable [13], this value of *QI* corresponds to a coil maximum temperature under protection heaters of ~250 K. In reality, taking into account the data in Fig. 12 and the fact that to accumulate this value of *QI* takes more than 0.1 s, the coil maximum temperature under protection heaters is even lower. Using a small dump resistor of ~2-10 mOhm noticeably reduces the *QI* and, thus, the maximum coil temperature [10].

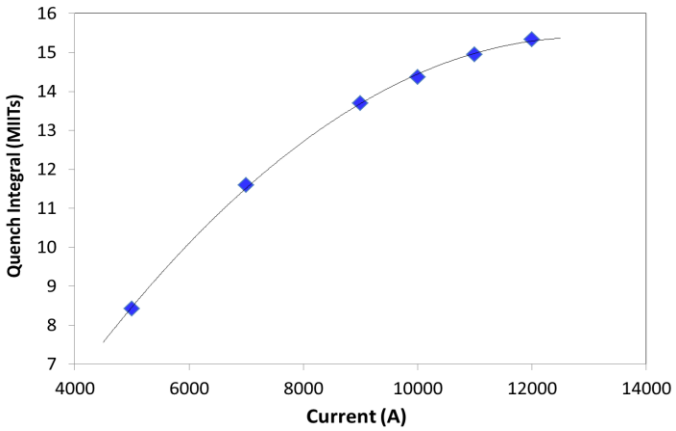

Fig. 13. Quench Integral vs. magnet current (MBHSM01).

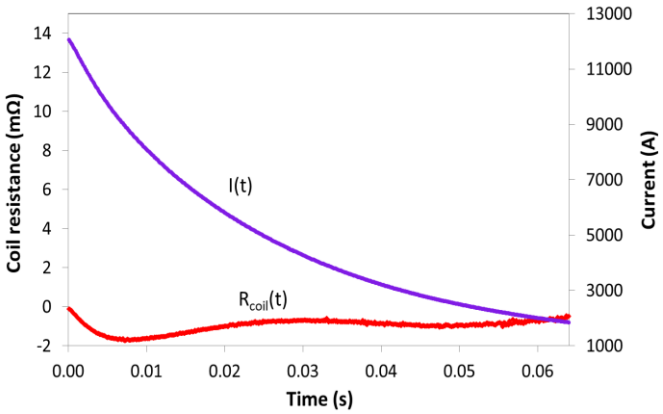

Fig. 14. Magnet current and resistance vs. time.

D. Quench-back effect

To observe the so called "quench-back" effect in the 11 T dipole, fast energy extraction tests were performed in dipole mirror MBHSM01 at various currents without the protection heaters. If present, this effect helps to distribute the magnet stored energy due to coil quench by AC losses in conductor. Fig. 14 shows the coil resistance variation during the magnet current decay. The negative value of coil resistance shows that the "quench-back" effect is not present in 11 T dipole coils made of cored cable at currents up to 12 kA.

E. Longitudinal quench propagation velocity

The quench propagation velocity along the cable in a coil is an important parameter to estimate the *QI* in the quench origin area and optimize the PH design. The measured and calculated using [15] data for the OL mid-plane (MP) turn and the IL pole turn are shown in Fig. 15. The quench propagation velocity in the OL mid-plane turn was measured using the spot heater. The cable under the spot heater was quenched at a power density of ~26 W/cm^2. The quench propagation velocity along the cable was determined using two different methods [10]. In Method A the slope of the voltage growth *dV/dt* between the voltage taps was used. In Method B the quench propagation velocity was defined as the ratio of the cable segment length L=100 mm to the measured time of the normal zone propagation between the voltage taps. The quench propagation velocity in the IL pole turn was estimated using the *dV/dt* slope during some training quenches. The OL-MP results from both methods are very consistent and in excellent correlation with calculations. The quench propagation velocity measured in IL-Pole turn is also in agreement with calculations. Quench velocity measurements in the inner-layer mid-plane turn using SH will continue.

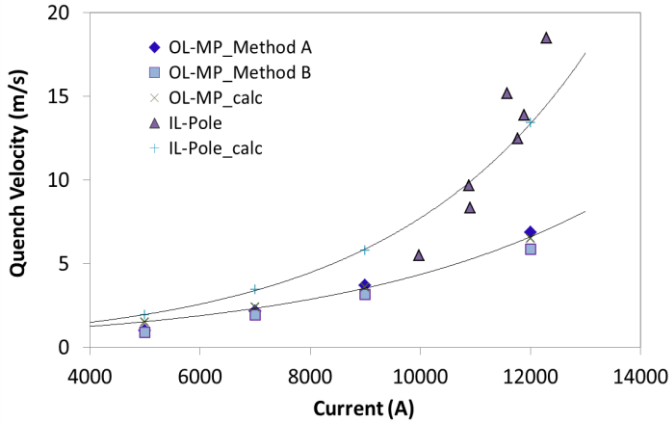

Fig. 15. Longitudinal quench velocity in coil (MBHSM01).

F. Radial quench propagation

Simulations [12] and heater studies in 11 T dipole models [13],[14] revealed that a quench propagates quite rapidly in the radial direction from OL to IL coil blocks, helping to distribute the magnet stored energy over a larger coil volume and, thus, to reduce the coil maximum temperature. Quench delay time was measured separately for coil OL and IL blocks at 4.5 K and 1.9 K. Quench delay time was determined as the time between the heater initiation and the voltage detection in the coil. Fig. 16 shows the quench delay time measured and calculated using [15] in both layers as a function of the magnet current at P_{AV}=50 W/cm^2. A reasonably good correlation between measurements and calculations for the IL is observed at all currents whereas the OL calculations are consistent with measurements only above 7 kA. At the lower currents the measured and calculated data diverge. This discrepancy could be associated with the effect of large contact thermal resistances between the heater strips, Kapton insulation and coil surface, which depend on the radial Lorentz force.

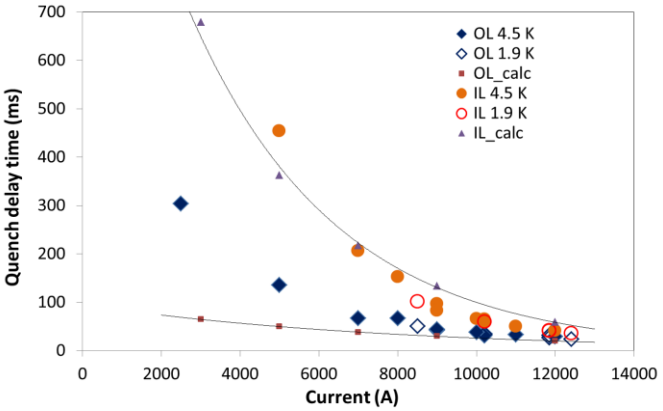

Fig. 16. Quench delay time in IL and OL vs. magnet current (MBHSP01, MBHSP02 and MBHSM01).

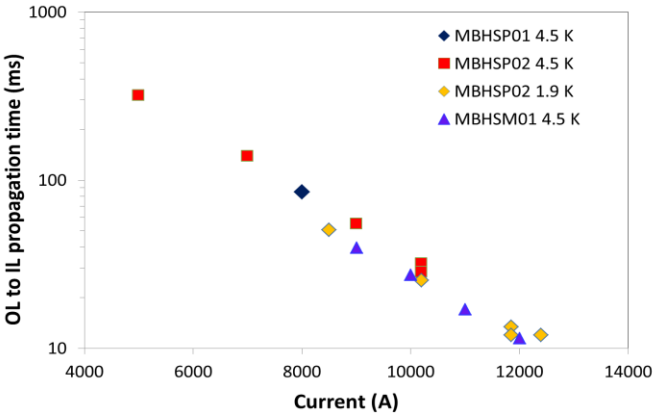

Fig. 17. Radial quench propagation time from OL to IL.

The quench propagation time between the coil layers was estimated as the time difference between the quench detection in the OL and IL of the coil. Fig. 17 shows this time difference vs. the magnet current. The results for similar heaters in dipole demonstrator MBHSP01 and in dipole model MBHSP02 are also shown, validating excellent heater performance reproducibility. In high currents close to the nominal LHC operation current this parameter is less than 20 ms.

G. Quench delay in HF and LF coil blocks

Two OL coil blocks are exposed to different magnetic fields and, thus, have different temperature margins and response times to the PH discharge. On the other hand, the width of the LF heater is smaller than the width of the HF heater resulting in the lower power density in the HF heaters than in the LF heaters (see section A). The measured and calculated combined effect on the quench delay time for HF and LF blocks vs. magnet current is shown in Fig. 18. At 12 kA the measured response time difference is ~30 ms, increasing at the lower currents, whereas the calculated value is more than a factor of

two smaller and reduces at lower currents. This discrepancy could also be related to the presence of large contact thermal resistances between the heaters and the coil. The observed difference of the response time in the HF and LF blocks could be reduced by adjusting the PH power in the HF and LF protection heaters, e.g. by optimizing the heater strip width, heater insulation thickness and gluing the heaters to the coil.

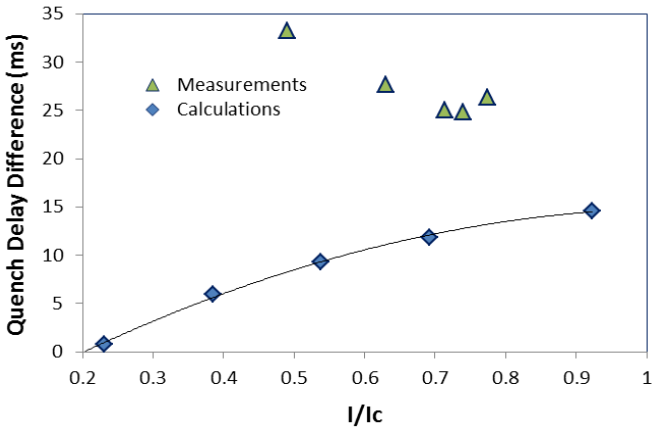

Fig. 18. Quench delay difference for the LF and HF outer-layer blocks vs. normalized magnet current (MBHSM01).

VI. Magnetic Measurements

Field quality measurements provide important information on the geometrical harmonics, coil magnetization, iron saturation and dynamic effects in 11 T dipole models [17], [18]. The data, obtained in single aperture configuration, are compared with simulations. Later they will be also compared with the results of magnetic measurements in the twin-aperture model to better understand the magnetic coupling between two apertures and possible asymmetry of magnet cross-section during assembly and operation.

The magnetic measurements were performed using two 16-layer probes based on the Printed Circuit Board (PCB) technology [19]. The typical rotational speed of the probe was 1 Hz. Field harmonic coefficients are defined by the formula

$$B_y + iB_x = B_1 10^{-4} \sum_{n=1}^{\infty} (b_n + ia_n) \left(\frac{x+iy}{R_{ref}} \right)^{n-1} ,$$

where B_x and B_y are the horizontal and vertical field components in the Cartesian coordinate system, and b_n and a_n are the $2n$-pole normal and skew harmonic coefficients at the reference radius R_{ref}=17 mm.

A. Coil magnetization and iron saturation effects

The measured magnet Transfer Function (*TF*), defined as *TF=B/I*, where *B* is the magnet bore field and *I* is the current, and normal sextupole (b_3) loops for MBHSP02 and MBHSP03 vs. the magnet current at 1.9 K for several current ramp rates are shown in Figs. 19 and 20. Dashed lines represent *TF* and b_3 loops, calculated for MBHSP02 using the 2D ROXIE model with magnetization data for RRP150/159 strand and iron yoke *B(H)* curve. The calculated b_3 loop was shifted up by 8 units to match the geometrical component in MBHSP02 (see Fig. 22).

The persistent current effect in the *TF* and b_3 is substantial in MBHSP02 and MBHSP03 at low currents due to large D_{eff} (~0.041 mm for RRP108/127 and ~0.036 mm for RRP150/169 [20], which is a factor of 6 to 7 larger than the Nb-Ti filament size in the MB magnets) and high J_c (factor of 2 to 3 higher than in the Nb-Ti strands used in MB magnets) of the Nb_3Sn RRP strand used in both models. There is a quite good correlation of the measured and calculated data for the persistent current effect at currents above 1.5 kA, shown in Figs. 19 and 20, and reported also in [21]. The ramp rate effect is small as expected for the cable with a resistive core.

The iron saturation effect in *TF* and b_3, seen at currents above 4 kA, is in general consistent with calculations based on the iron magnetic properties and geometry used in these models [22]. At high currents the difference between calculated and measured *TF* is less than 1.5% and the difference for Δb_3 is less than 6 units.

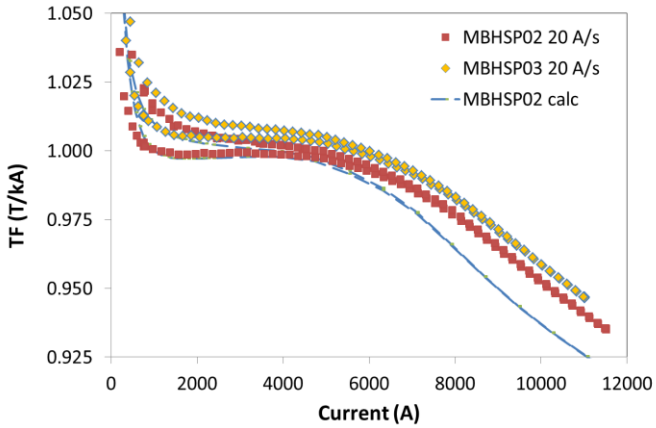

Fig. 19. Transfer function *TF* vs. magnet current.

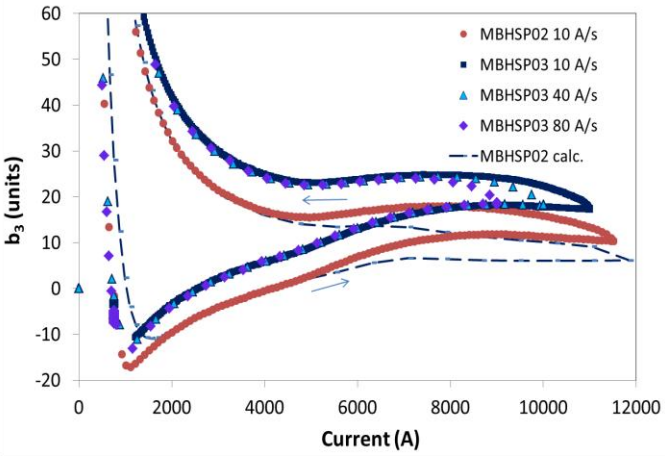

Fig. 20. Sextupole b_3 vs. magnet current.

B. Sextupole decay

The measured b_3 decay at the LHC injection porch in MBHSP02 and MBHSP03 is shown in Fig. 21. In both models the b_3 decay is reproducible and quite large, ~4-7 units, unlike in previously tested Nb_3Sn dipoles [17], [23]. A possible cause of the unexpectedly large b_3 decay could be local core damage (e.g. in the coil ends where the cable experiences large and complex bending deformations), which could lead to local reduction of the interstrand resistance in these areas. The effect in this case could be reduced by reducing the core width while keeping the ramp rate effects on the acceptable level.

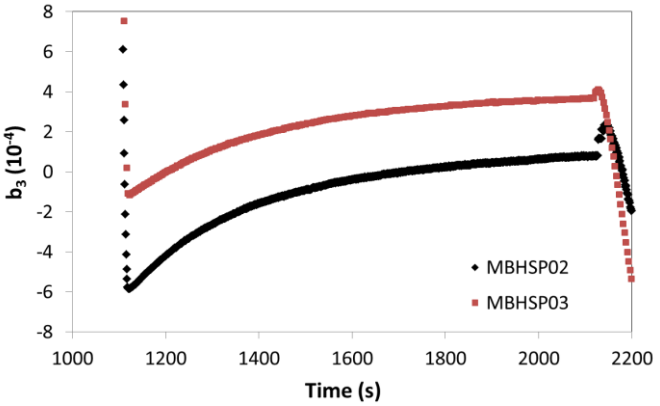

Fig. 21. Sextupole b_3 decay at injection current 760 A.

C. Geometrical harmonics

Fig. 22 shows the measured geometrical harmonics at a current of 3.5 kA in the magnet center for both models. All the higher order harmonics (n>3) are small, ~1 unit or less. The value and difference of the low order harmonics in the two tested models are rather large due to the variations of the coil size during fabrication, and of assembly shims used for coil pre-stress. In production magnets these harmonics could be reduced by stabilizing the coil geometry variations.

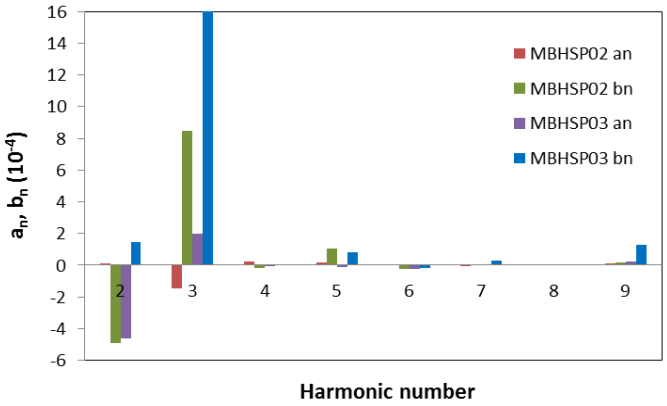

Fig. 22. Geometrical normal b_n and skew a_n field harmonics.

VII. 2-in-1 Model Assembly

In a twin-aperture configuration, two collared coils are installed inside a vertically split iron yoke with an iron spacer in between, and surrounded by a thick stainless steel skin. Two thick stainless steel end plates, welded to the skin, restrict the axial motion of both collared coils.

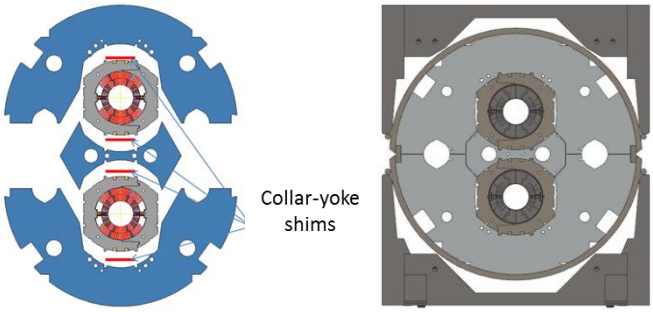

Fig. 23. Twin-aperture 11 T dipole model assembly shimming (left) and cold mass welding (right) schemes.

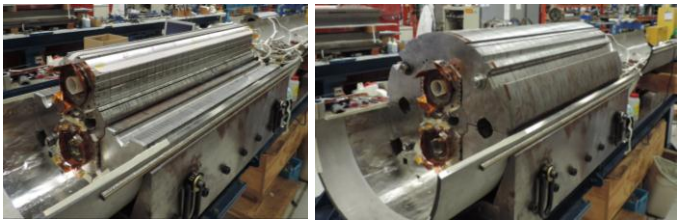

Fig. 24. Assembly of two collared coils with the iron yoke and skin (left) and the 2-in-1 magnet cold mass inside the bottom half-skin (right).

Two collared coils, MBHSP02 and MBHSP03, are used in the first twin-aperture dipole model. Based on the test results, the collared coil of MBHSP03, was re-collared with slightly larger radial shim to increase the coil pre-stress before using in the twin-aperture dipole model. The assembly and shimming scheme of the twin-aperture 11 T dipole model is shown in Fig. 23 (left). The longitudinal midplane shims, the same as in MBHSP03, provide some small collared coil bending to keep contact between the collar and the yoke after cooling down. The cold mass compression before skin welding is shown in Fig. 23 (right). The assembly of the first twin-aperture dipole model is in progress. Fig. 24 shows the assembly of two collared coils inside the iron yoke and of the 2-in-1cold mass inside a half-skin.

VIII. Conclusion

The work on the development of the 11 T Nb_3Sn dipole for the LHC upgrades continues at FNAL in collaboration with CERN. Seven 1 m long coils were fabricated since 2012. Four coils were assembled in two collared coil assemblies and tested in a single-aperture configuration. Both collared coils were trained above the nominal operation field of 11 T to ~11.6 T at 1.9 K, or 97% of the dipole design field of 12 T. Important information on the magnet quench performance and field quality, including geometrical harmonics, coil magnetization, iron saturation and dynamic effects in 11 T dipole models, was obtained. These collared coils are being assembled in the first twin-aperture dipole model. One of the tested collared coils was re-collared with slightly larger radial shim to increase the coil pre-stress before using it in the twin-aperture model. The assembly of the first twin-aperture dipole model is in progress. Model test is planned in December 2014.

One 1 m long coil was tested in the dipole mirror configuration, which had been developed at FNAL to assess the role of coil pre-load and measure the coil quench protection parameters. The improved quench performance of this coil allowed clarifying the conductor performance degradation in the first 11 T dipole models. Experimental studies of key quench protection parameters, such as protection heater efficiency, quench propagation in the coil in various directions and coil heating during quench, provided an important input to the 11 T dipole quench protection system design and performance optimization.

Acknowledgment

The authors thank the staff of FNAL Technical Division for contributions to magnet design, fabrication and test.

REFERENCES

[1] L. Bottura *et al*., "Advanced Accelerator Magnets for Upgrading the LHC," *IEEE Trans. on Appl. Supercond*., Vol. 22, Issue 3, 2012, Art. No. 4002008.

[2] A.V. Zlobin *et al*., "Development of Nb_3Sn 11 T Single Aperture Demonstrator Dipole for LHC Upgrades," Proc. of PAC'2011, NYC, 2011, p. 1460.

[3] A.V. Zlobin *et al*., "Development and test of a single-aperture 11T Nb_3Sn demonstrator dipole for LHC upgrades,**"** *IEEE Trans. on Appl. Supercond*., Vol. 23, N 3, 2013, Art. No. 4000904.

[4] A.V. Zlobin *et al*., "Status of the 11 T 2-in-1 Nb_3Sn Dipole Development for LHC," Proc. of IPAC'2014, Dresden, June 2014.

[5] A.V. Zlobin *et al*., "Testing of a Single 11T Nb_3Sn Dipole Coil using a Magnetic Mirror Structure," Proc. of IPAC'2014, Dresden, June 2014.

[6] M. Karppinen *et al*., "Design of 11 T Twin-Aperture Nb_3Sn Dipole Demonstrator Magnet for LHC Upgrades," *IEEE Trans. on Appl. Supercond*., Vol. 22, N 3, 2012, Art. No. 4901504.

[7] E. Barzi *et al*., "Development and Fabrication of Nb_3Sn Rutherford Cable for the 11 T DS Dipole Demonstration Model," *IEEE Trans. on Appl. Supercond.*, Vol. 22, Issue 3, June 2012, Art. No. 6000805.

[8] E. Barzi *et al*., "Superconducting Strand and Cable Development for the LHC Upgrades and Beyond," *IEEE Trans. on Appl. Supercond*., Vol. 23, Issue 3, June 2013, Art. No. 6001112.

[9] A.V. Zlobin *et al*. "Design and Fabrication of a Single-Aperture 11T Nb_3Sn Dipole Model for LHC Upgrades," *IEEE Trans. Appl. Supercond*., Vol. 22, N 3, 2012, Art. No. 4001705.

[10] A.V. Zlobin *et al*., "Quench Protection Studies of 11T Nb_3Sn Dipole Coils," Proc. of IPAC'2014, Dresden, June 2014.

[11] F. Savary et al., "Design, assembly and test of MBHSM101, a 2-m long practice model made of a single coil wound with Nb_3Sn cable at CERN," *IEEE Trans. Appl. Supercond*. submitted for publication.

[12] A.V. Zlobin, I. Novitski, R. Yamada, "Quench Protection Analysis of a Single-Aperture 11T Nb_3Sn Demonstrator Dipole for LHC Upgrades," Proc. of IPAC'2012, New Orleans, Louisiana, USA, p.3599.

[13] G. Chlachidze, *et al*., "Experimental results and analysis from 11T Nb_3Sn DS dipole," FERMILAB-CONF-13-084-TD, and WAMSDO'2013 at CERN, January 2013, CERN-2013-006.

[14] G. Chlachidze *et al*., "Quench protection study of a single-aperture 11T Nb_3Sn demonstrator dipole for LHC upgrades," *IEEE Trans. on Appl. Supercond.*, Vol. 23, Issue 3, June 2013, Art. No. 4001205.

[15] S. Izquierdo Bermudez, H. Bajas, L. Bottura , "Quench Modeling in High-Field Nb_3Sn Accelerator Magnets," 25th International Cryogenic Engineering Conference and the International Cryogenic Materials Conference in 2014, ICEC 25–ICMC 2014, Physics Procedia, 2014.

[16] H. Bajas *et al*., "Quench Analysis of High Current Density Nb_3Sn Conductors in Racetrack Coil Configuration," *IEEE Trans. Appl. Supercond*. submitted for publication.

[17] N. Andreev *et al*., "Field quality measurements in a single-aperture 11T Nb_3Sn demonstrator dipole for LHC upgrades," *IEEE Trans. on Appl. Supercond*., Vol. 23, Issue 3, June 2013, Art. No. 4001804.

[18] G. Chlachidze *et al*., "Field quality study of a 1-m Long single-aperture 11T Nb_3Sn dipole model for LHC upgrades," *IEEE Trans. on Appl. Supercond*., Vol. 24, Issue 3, June 2014, Art. No. 4000905.

[19] J. DiMarco *et al*., "Application of PCB and FDM Technologies to Magnetic Measurement Probe System Development," *IEEE Trans. on Appl. Supercond*., Vol. 23, Issue 3, June 2013, Art. No. 9000505.

[20] E. Barzi *et al*., "Progress in Nb_3Sn RRP Strand Studies and Rutherford Cable Development at FNAL," *IEEE Trans. on Appl. Supercond*., Vol. 24, Issue 3, June 2014, Art. No. 6000808.

[21] X. Wang *et al*., "Field errors induced by persistent current in high-field superconducting accelerator magnets," *IEEE Trans. Appl. Supercond*. submitted for publication.

[22] B. Auchmann *et al*., "Magnetic Analysis of a Single-Aperture 11T Nb_3Sn Demonstrator Dipole for LHC Upgrades," Proc. of IPAC2012, New Orleans, Louisiana, USA, p. 3596.

[23] E. Barzi *et al*., "Field Quality of the Fermilab Nb_3Sn Cos-theta Dipole Models," Proc. of EPAC2002, Paris, June 3-7 2002, p.2403.

[24] A.V. Zlobin *et al*., "Quench performance of a 1-m Long single-aperture 11T Nb_3Sn dipole model for LHC upgrades," *IEEE Trans. on Appl. Supercond*., Vol. 24, Issue 3, June 2014, Art. No. 4000305.